The Synthesis and Magnetic Properties of a Nanostructured Ni-MgO System

J. Narayan, Sudhakar Nori, S. Ramachandran, and J.T. Prater

We have investigated the magnetic properties of the Ni-MgO system with an Ni concentration of 0.5 at.%. In as-grown crystals, Ni ions occupy substitutional Mg sites. Under these conditions the Ni-MgO system behaves as a perfect paramagnet. By using a controlled annealing treatment in a reducing atmosphere, we were able to induce clustering and form pure Ni precipitates in the nanometer size range. The size distribution of precipitates or nanodots is varied by changing annealing time and temperature. Magnetic properties of specimens ranging from perfect paramagnetic to ferromagnetic characteristics have been studied systematically to establish structure-property correlations. The spontaneous magnetization data for the samples, where Ni was precipitated randomly in MgO host, fits well to Bloch's $T^{3/2}$-law and has been explained within the framework of spin wave theory predictions.

INTRODUCTION

Magnesium oxide (MgO) is an interesting host material in which cation sites can be selectively doped with magnetic ion impurities such as Ni, Co, Cu, and Fe. Such embedded metallic precipitates, when reduced in size to nanometer scale in an immiscible conducting or insulating medium, capture a rich variety of physical properties such as giant magnetic and transport properties due to spin-dependent scattering and a high degree of spin-polarized current transport ideal for spintronics-based applications.[1–4] Room temperature ferromagnetism (RTFM) associated with a giant magnetic moment and a high Curie temperature (T_c) has been reported in Co-doped CeO_2 thin films, a high-*k* dielectric material belonging to the diluted magnetic semiconductor/insulator (DMS/DMI) systems.[5] Systematic changes in the size distribution of metal precipitates in MgO exhibit optical spectra (near 2.2–5.0 eV) of these materials, making them ideal candidates for high-temperature solar absorber applications with enhanced mechanical properties.[6] When these impurities are in a doubly ionized state, they have unpaired electrons in the 3d-shell, such as Ni^{++} ($3d^8$), Co^{++} ($3d^7$), Cu^{++} ($3d^9$), and Fe^{++} ($3d^6$). These partially filled 3d shells have unpaired spins that result in a magnetic moment. When these ions are randomly distributed in the lattice in a noninteracting fashion, there is no net magnetic moment and the system behaves as a perfect paramagnet. At low magnetic fields these paramagnetic materials exhibit linear M vs. H characteristics with no coercivity.

By subtractive coloration involving internal reduction, it is possible to reduce Ni^{++} and cluster them into metallic precipitates. By controlling the time and temperature of the reduction treatment, we are able to vary and control the fraction of nickel that enters into substitutional sites and nanoprecipitates (nanodots or nanoclusters) and their size distribution. In this study, we have investigated structure-property correlations in three sets of samples: all nickel on substitutional (Mg sites); a fraction on substitutional sites and the rest in metallic precipitates; and all nickel on precipitates (nanodots). Here we report a detailed set of results of magnetization of the Ni-doped MgO system as a function of temperature, applied magnetic field strength, and orientation or crystal direction with respect to the applied magnetic field direction. Magnetic properties, M vs. H and M vs. T, are correlated with the nature of Ni ion and cluster distribution in these samples. These nanodots have a great potential for information storage and for functional magnetic sensors. The magnetic properties arise

How would you…

…describe the overall significance of this paper?

This paper describes the changes in magnetic properties that occur in Ni-doped MgO (a dilute magnetic material) as the Ni moves from solid solution to nanoprecipitates. In the Ni-doped MgO system, we can change the magnetic properties systematically by manipulating time and temperature of annealing treatments. This system's ferromagnetism at room temperature offers potential for nanomagnetics and information-storage applications.

…describe this work to a materials science and engineering professional with no experience in your technical specialty?

We have created a novel Ni-doped MgO system, where it behaves as a perfect paramagnet (noninteracting moments), if Ni^{++} ions are distributed uniformly and substitutionally in the MgO matrix. By an internal reduction treatment at a high temperature, we induce clustering of nickel atoms and these precipitates exhibit ferromagnetism below the blocking temperature.

…describe this work to a layperson?

In the Ni-doped MgO system, the Ni can be controlled precisely from individual ions to nanoparticles and clusters. Correspondingly, the magnetic properties change from being a perfect paramagnet to a ferromagnet. The clusters exhibit ferromagnetism at and above room temperature where Ni nanoparticles are embedded epitaxially into the MgO matrix. If a nanoparticle can contain one bit of information, we can easily store over a Terabit of information in a single chip.

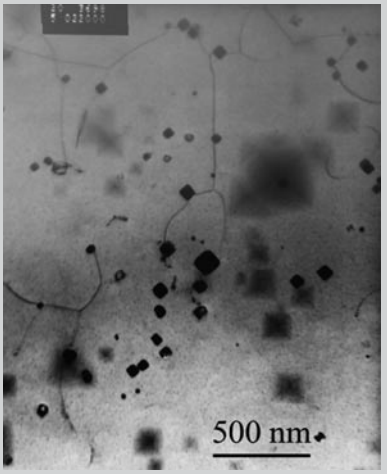

Figure 1. A transmission electron micrograph showing the distribution of Ni nanoclusters in MgO matrix.

predominantly due to the nickel in the divalent state that has an electronic configuration of $t_{2g}^{6}e_{g}^{2}$. See the sidebar for experimental details

RESULTS AND DISCUSSION

Figure 1 shows a transmission-electron-microscopy (TEM) micrograph of Ni-doped MgO after the internal reduction treatment, displaying a distribution of metallic precipitates. A comparative study on as-grown Ni-doped MgO showed no contrast as all the Ni ions occupy substitutional sites. Detailed high-resolution TEM studies showed the Ni/MgO interface to be atomically sharp without any interfacial reaction. The size distribution of the precipitates ranged from 10 to 100 nm with an average size of 50 nm as shown in Figure 2. From the diffraction studies, we deduced the following precipitate (p) and matrix (m) orientation relationship: $[11\bar{1}]_p \parallel [100]_m$ and $[1\bar{1}0]_p \parallel [010]_m$. The role of orientation relationship on the anisotropy of magnetic properties of these materials will be discussed later in this paper.

The crystals with substitutional Ni displayed paramagnetic properties throughout the entire temperature range, as shown in Figures 3 and 4. This linear M vs. H plotted in Figure 3 is a typical characteristic of a perfect paramagnet. The temperature dependence of the magnetic susceptibility of the Ni-MgO substitutional sample is plotted in Figure 4.

The solid line is the fit to the Curie's

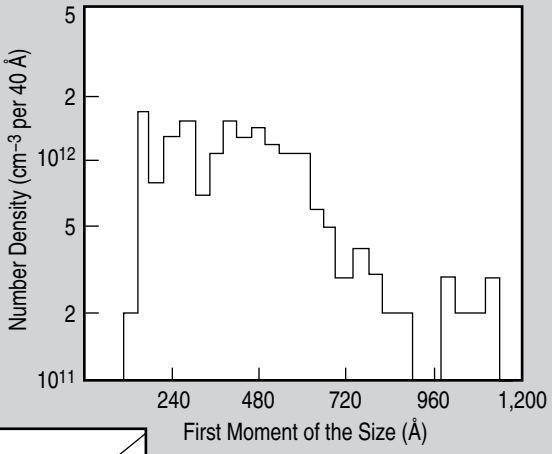

Figure 2. The size distribution (first moment of the size versus number density) of the Ni nanoparticles in the host MgO matrix.

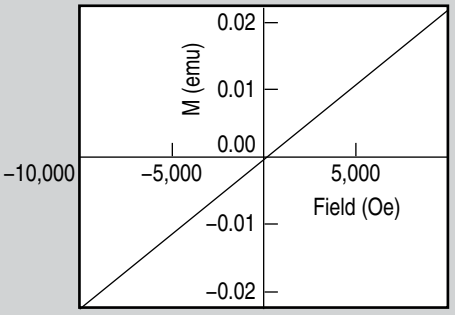

Figure 3. The field-dependent magnetization of Ni-MgO sample measured at 5 K with Ni in the substitutional sites.

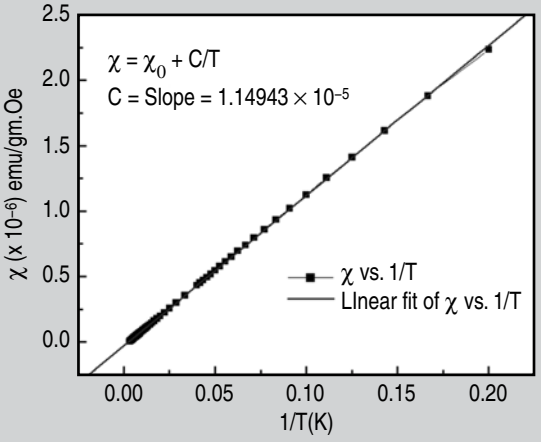

Figure 4. The temperature dependence of the magnetic susceptibility of the Ni-MgO substitutional sample. The solid line is the fit to the Curie's law clearly illustrating the paramagnetic behavior of the sample.

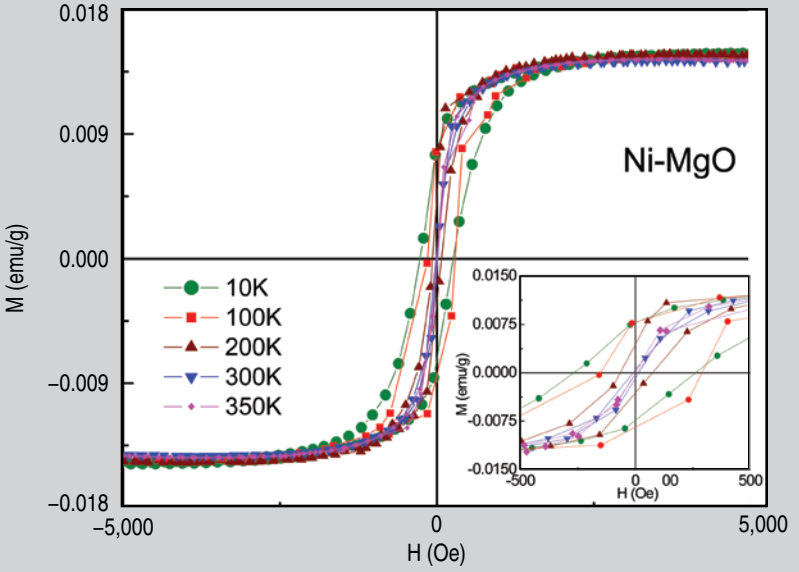

Figure 5. Isothermal field-dependent magnetization curves up to 5,000 Oe for the fully Ni-MgO precipitated sample at selected temperatures in the range 10–350 K. Plotted in the bottom right inset are the M-H loops in the range ± 500 Oe to show the hysteresis and coercivity in a more discernible way.

Table I. Important Parameters such as Saturation Magnetization (M_s), Magnetization at 10 kOe, Remnant Magnetization (M_R), Coercive Field (H_c) and the Initial Saturating Field (H_s) Calculated from the Temperature-Dependent Magnetization of Ni-MgO

T (K)	5 K	10 K	100 K	200 K	300 K	350 K
M_s (emu/g)	1.50×10^{-2}	1.49×10^{-2}	1.48×10^{-2}	1.47×10^{-2}	1.44×10^{-2}	1.43×10^{-2}
M_{10kOe}(emu/g)	1.45×10^{-2}	1.43×10^{-2}	1.35×10^{-2}	1.35×10^{-2}	1.28×10^{-2}	1.27×10^{-2}
M_R (emu/g)	8.18×10^{-3}	7.98×10^{-3}	7.69×10^{-3}	4.49×10^{-3}	1.62×10^{-3}	$<1.0 \times 10^{-5}$
H_c (Oe)	315.0	281.0	216.0	71.0	15.0	6.0
H_s (Oe)	5,700	5,250	4,100	4,000	3,830	3,750

law clearly illustrating the paramagnetic behavior of the sample. On the other hand, the MgO crystals with Ni precipitates displayed interesting ferromagnetic properties with coercivity (as measured by the intercepts in the H-axis of M (H) curves) up to temperatures as high as 350K. The M vs. H results for 10, 100, 200, 300, and 350 K up to H = ±5,000 Gauss are shown in Figure 5, and the inset shows the data for H = ±500 Gauss. The intercept in the –H axis is a measure of coercivity and associated ferromagnetism. Plotted in the bottom inset are the M vs. H loops in low fields (from –500 to +500 Oe) to decipher the presence of ferromagnetic behavior up to 350 K. Both coercive and saturating field decreased as the temperature increases from 10 K to 350 K. The monotonic decrease of coercivity with the increase in temperature and its exact temperature dependence is given in Equation 4. These characteristics are consistent with the properties expected for nanostructured systems. Table I provides a summary of critical parameters, including saturation magnetization (M_s), remnant magnetization (M_R), coercivity (H_c), and the initial saturating field (H_s).

The temperature dependence of the magnetization of the Ni-doped MgO sample has been measured both under zero-field-cooled (ZFC) and field-cooled (FC) conditions in the range of 5 to 350 K. The magnetization was measured for different magnetic fields of 500, 5,000, and 10,000 Oe, as shown in Figures 6, 7, and 8, respectively. It is evident from Figures 6 and 7 that the ZFC and FC magnetization curves show a bifurcation. The bifurcation temperature sometimes referred to as irreversibility temperature (T_{irr}) in the literature, decreased from around 330 K to 250 K as the field strength increased 500 Oe to 5,000 Oe. Upon further increase in the magnetic field strength to 5 or 10 kOe the ZFC and FC magnetization curves merge into a single curve. M_{ZFC} is related to M_{FC} according to the following expression,

$$M_{ZFC} \approx (H_A M_{FC})/(H_A + H_c) \qquad (1)$$

where H_A and H_c are the applied and coercive fields, respectively. For high values H_A (>5,000 Oe) Equation 1 reduces to $M_{ZFC} \approx M_{FC}$, that is consistent with the experimental M (T) data plotted in Figures 6–8. It is clear from the plots that those MgO crystals in which Ni is precipitated as clusters exhibit room-temperature ferromagnetism (FM). Actually, the M (T) plots suggest a transition from the FM state to PM above 300 K and the transition temperature (T_c) could be well above 300 K.

Here, we have attempted to interpret the experimentally observed data of both H_c as well as the spontaneous M in the light of the Stoner–Wolfforth model[10] developed for the noninteracting single domain particles that show shape or magnetocrystalline anisotropy and obey Bloch's spin wave theory,[11] respectively. Spin waves or magnons of an ordered magnetic lattice arise essentially due to low-energy collective excitations.[12] Isothermal M versus $1/H^2$ is plotted in Figure 9 for different temperatures to determine the saturation magnetization. Here M_s has been extracted by extrapolating the magnetization data to infinite fields. Spin wave theory accounts well for ferromagnets in the temperature range $T < T_c$ and gives a good description of the magnetization behavior. According to Bloch's law, the temperature dependence of saturation magnetization follows

$$M = M_s (1–BT^{3/2}) \qquad (2)$$

where B is the spin wave constant or Bloch's constant. We have plotted the saturation magnetization (M_s) vs. $T^{3/2}$ using Equation 2 in Figure 10. The solid line in the plot represents a linear fit to the data and confirms that the data is in accordance with the predictions of the Bloch's spin wave theory. The spin wave constant (B) estimated from the above analysis is ~2.1×10^{-5} $K^{2/3}$, which is about an order of magnitude larger than that of bulk Ni[13] where it is assumed that only 0.5 at.% of Ni contributes to the total amount. Similar results had been reported by Xiao and Chien for the case of ensembles of ultra-fine particles of Fe and in granular FeO-SiO_2 solids[14,15] and in ultra-fine Ni particles where the experimentally obtained spin wave constant values are larger by an order of magnitude than bulk Ni.[20] The large values of B in Bloch's equation are essentially a manifestation of the size effects of the Ni nano-precipitates. The Ni nano-clusters affecs the spin waves by softening

EXPERIMENTAL DETAILS

Ni-doped MgO crystals have been synthesized using an arc fusion technique, where the mixture of NiO and MgO is melted and crystals grown in a bulk form.[7–9] In as-grown crystals, Ni^{++} ions occupy substitutional Mg^{++} sites. These crystals exhibit green color emission at room temperature. We utilized an internal reduction (subtractive coloration) technique at high temperatures to reduce Ni^{++} and cluster them into metallic nickel precipitates. It is surmised that during the internal reduction treatment, oxygen vacancies are created, which can trap electrons and be transferred to Ni ions to reduce their charges. These neutral nickel ions and vacancy complexes cluster to form metallic precipitates. The characteristics of nickel precipitates and their size distribution were investigated by transmission electron microscopy techniques. Magnetic properties of as-grown and reduced crystals were characterized in the temperature range of 10–350 K. The temperature and field dependence of magnetization were measured using an MPMS-XL superconducting quantum interference device at temperatures of 5–350 K and a physical property measurement system in conjunction with a vibrating sample magnetometer attachment. Hysteresis measurements were performed by scanning the magnetic fields from –20 kOe to +20 kOe at temperatures ranging from 5 to 350 K.

the spin wave spectrum with a cut off for wave lengths that are larger than the physical dimensions of the clusters.[14]

The blocking temperatures observed in the ZFC measurements also show a similar variation. This is a characteristic feature of superparamagnetic behavior arising due to the presence of Ni nanoclusters. Thus, from a detailed magnetic characterization of both types of crystals we can infer that the crystals having substitutional Ni show perfect paramagnetism because of the absence of defects like vacancies to couple the moments of the unpaired d electrons in Ni. But in the case of crystals with Ni precipitates the ferromagnetic properties arise due to the Ni clusters and not as an intrinsic property of the MgO host itself. Therefore, it is highly desirable that in order to induce room-temperature ferromagnetism in substitutionally doped oxide based material systems the presence of defects like vacancies is highly critical. We have introduced defects by high energy ion implantation (100 MeV Ar^+ ions) and found ferromagnetic behavior at room temperature in Ni and Co doped MgO single crystals and thin films.[2]

The magnetic measurements (M (H) and M (T)) from samples, where some of the Ni is in substitutional sites and the rest in precipitates, are shown in Figures 11 and 12. Figure 11 shows the M vs. H curve at 5 K, and the inset shows ferromagnetic characteristics with a coercivity of 65 Oe in these samples. However, M does not saturate up to a field of 20 kOe, which is a clear indication that there is a paramagnetic signal superimposed on the ferromagnetic signal. To probe these characteristics further, M vs. T measurements under FC and ZFC were carried out and the results are shown in Figure 12. These characteristics can be rationalized by mixing the paramagnetic (obeying Curie–Weiss law) and ferromagnetic/super paramagnetic behavior (following a Langevin function) with a blocking temperature above 300 K.

The super paramagnetic contribution for an isotropic crystal is of the form

$$M = M_s[\coth(x) - 1/x] \qquad (3)$$

where $x = (\mu_0\, mH_m/kT)$, μ_0 is the permeability of free space, M is the average magnetization in the direction of external field H, $H_m = H + \alpha M$ is the effective field, M_s is the saturation magnetization, m is the magnetic moment, and α is the self-coupling coefficient. When x is large the term inside the bracket becomes a constant. Therefore, at low temperatures paramagnetic Curie–Weiss behavior dominates. At high temperatures (but below the blocking temperature) the superparamagnetic/ferromagnetic component dominates, and we observe the characteristics of Equation 3, as shown in Figure 12.

The field-dependent magnetization of the NiMgO system is also sensitive to the orientation of the sample with respect to the applied field. The magnetizations measured at 5 and 300 K of the sample in the transverse field are compared in Figure 13. Plotted in Figure 14 are the room-temperature magnetization curves measured for both transverse as well as longitudinal orientations. This is consistent with the orientation relationship of precipitate (p) with matrix (m): $[11\bar{1}]_p \parallel [100]_m$ and $[1\bar{1}0]_p \parallel [010]_m$ as determined from electron diffraction studies.

The monotonic decrease of H_c with the increase in temperature (from 315.0 Oe at 5 K to 6.0 Oe at 350 K) is due to the superparamagnetism that sets in at higher temperatures. For noninteracting nanosized particle systems, the coercivity is indeed a function of temperature and varies as[16–19]

$$H_c = H_0\,(1–(T/T_B)^{1/2}) \qquad (4)$$

where T_B is known as blocking temperature and is related to the magnetic anisotropy energy of the nanoprecipitates. The average size of the Ni clusters can be estimated with the knowledge of the blocking temperature of the system using Equation 5,

$$25\, k_B T_B = K_u V \qquad (5)$$

where K_u is the uniaxial anisotropy constant and V being the volume of the precipitate. For a T_B of 350 K the average size of the Ni clusters in MgO is about 30 nm. That is in good agreement with values obtained from TEM studies and the size distribution analysis (see Figures 1 and 2) where the average Ni cluster size is estimated to be ~50 nm. Using Equation 5 we have calculated and then plotted the variation of the blocking temperature (T_B) with the average diameter (<d>) of the precipitates of Ni along with other systems (NiPt, FePt, and Fe) in Figure 15. The coercivity (H_c) of the Ni nanoparticles also relates to the saturation moment (M_s) as[12]

$$H_c = 2K_u/M_s – (2/M_s)(25k_BK_u/V)^{1/2}T^{1/2} \qquad (6)$$

where M_s is the saturation magnetic moment per unit volume and K_u is the uniaxial anisotropy constant which is 5×10^4 erg/cm^3. Here the moment per unit volume has been estimated to be about 12.46 emu/cm^3 by converting the magnetic moment values from Table I (expressed emu/g) and by considering approximately one half a percent of the Ni contributing to the total recorded magnetization. For an M_s of 12.46 emu/cm^3 a quick calculation using Equation 6 for the coercivity may be estimated as 4.5×10^3 Oe which is about an order of magnitude greater than that of the bulk Ni value[13–16,20] and illustrates clearly the importance of the reduced size effects of the system. It should be noted that the enhanced values of coercivity estimated here (using Equation 6) are consistent with the values discussed earlier in the text for the spin wave constant (B) values for the Ni nanoprecipitates which are also about an order of magnitude higher than that of the bulk Ni. This shows that the Ni precipitates are clearly in the single-domain regime which can lead to higher values of coercivity than the bulk counterpart. Similar behavior has also been observed in the case of ultrafine Ni particles where the observed spin wave values are larger than the bulk Ni[20] and particles of Fe[14,15] and in granular FeO-SiO_2 solids.[16]

CONCLUSIONS

We have investigated the magnetic properties of the Ni-doped MgO system with an Ni concentration up to 0.5 at%. As-grown crystals with Ni in substitutional sites were observed to display paramagnetic behavior. Upon internal reduction treatment, Ni clustered into metallic precipitates and the system underwent a transition to ferromagnetic/superparamagnetic behavior. With an average size of 50 nm of Ni nanoparticles/nanodots, the system showed a blocking temperature well above 300

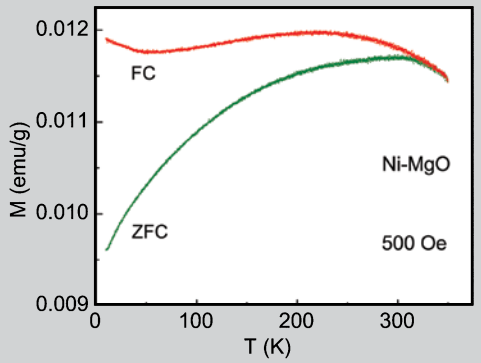

Figure 6. The temperature dependence of the dc magnetization data plotted for the fully Ni-MgO precipitated sample recorded in an applied magnetic field of 500 Oe. Both zero-field cooled (ZFC) and field-cooled (FC) magnetization curves are shown in the temperature range from 10–350 K.

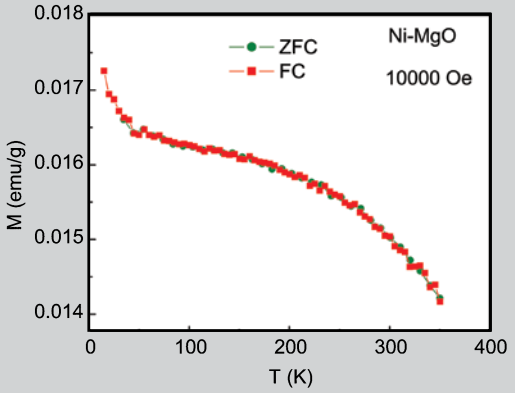

Figure 8. ZFC and FC magnetization curves as a function of temperature plotted for the fully Ni-MgO precipitated sample in a magnetic field of 10,000 Oe showing the complete merger over the entire temperature range from 10–350 K.

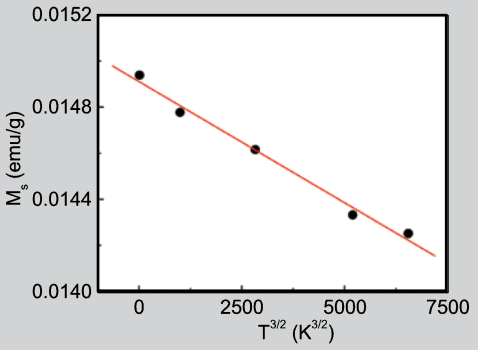

Figure 10. Saturation magnetization obtained from Figure 8 is plotted versus $T^{3/2}$. The solid line in the plot represents a linear fit to the data using $M = M_s (1\text{-}BT^{3/2})$. The spin wave constant (B) estimated from the above analysis is ~2.1×10^{-5} $K^{2/3}$.

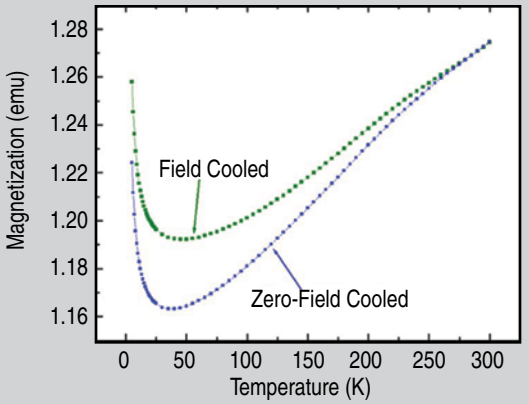

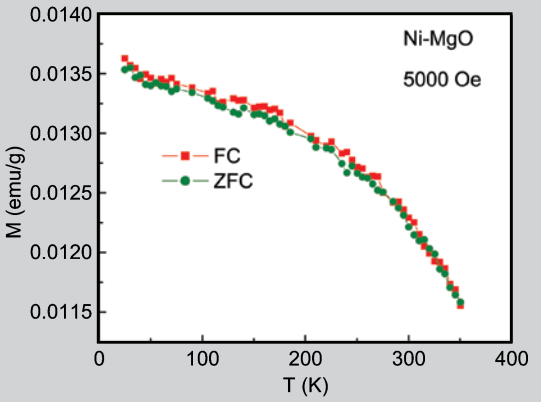

Figure 7. M vs. T curves plotted for the fully Ni-MgO precipitated sample in a magnetic field of 5,000 Oe. Both ZFC and FC magnetization curves are shown in the temperature range from 10–350 K.

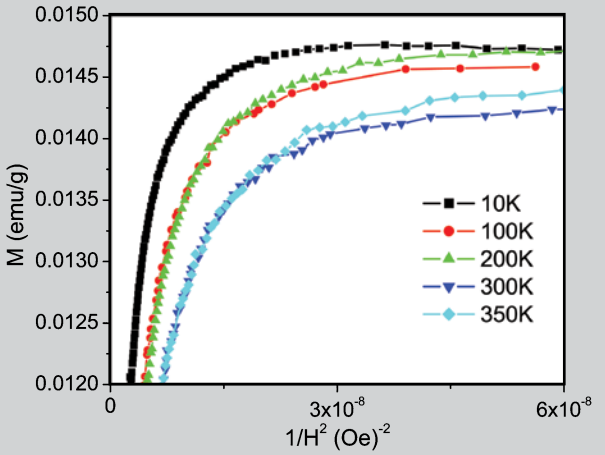

Figure 9. Isothermal spontaneous magnetization (M) versus $1/H^2$ plotted for different temperatures for the fully precipitated sample. The saturation magnetization (M_s) is extracted by the linear extrapolation of the magnetization data on to the y-axis as described in the text.

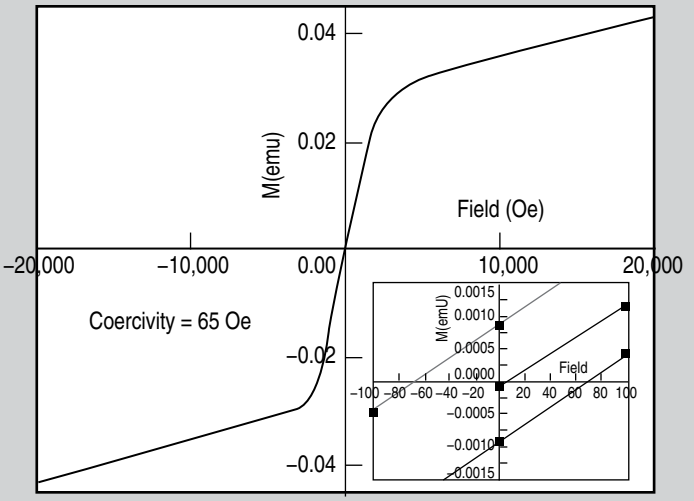

Figure 11. The field-dependent magnetization at 5 K for the Ni-MgO sample with Ni in the form of precipitates as well as in the substitutional sites showing clearly the non-saturation of the magnetization even in fields as high as 20,000 Oe illustrating the superparamagnetic behavior of the sample. The inset shows the coercivity of the sample to be about 65 Oe.

Figure 12. ZFC and FC magnetization curves as a function of temperature (5–300 K) for the Ni-MgO sample with Ni in the form of precipitates as well as in the substitutional sites.

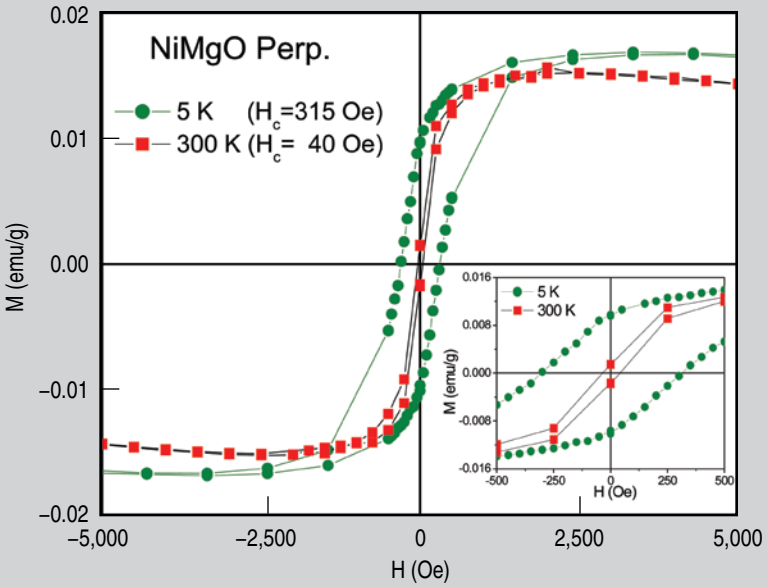

Figure 13. The field-dependent magnetization of the fully Ni-MgO precipitated sample at 5 and 300 K measured in a transverse field. The inset shows the hysteresis and the coercivity values varying from 315 Oe at 5 K to 40 Oe at room temperature.

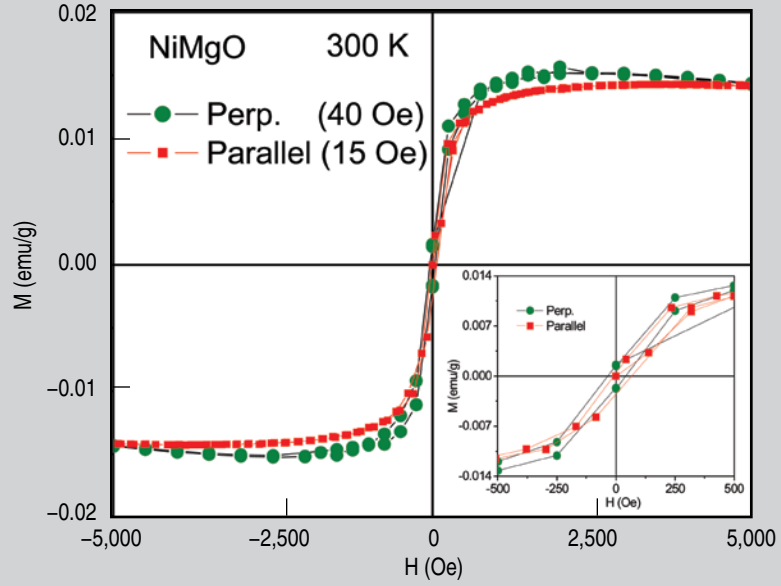

Figure 14. The field-dependent magnetization of the fully Ni-MgO precipitated sample with magnetic field applied in transverse and longitudinal (parallel) directions with respect to the sample measured at 300 K. The inset shows the coercivity values of 40 Oe and 15 Oe for the transverse and longitudinal directions respectively.

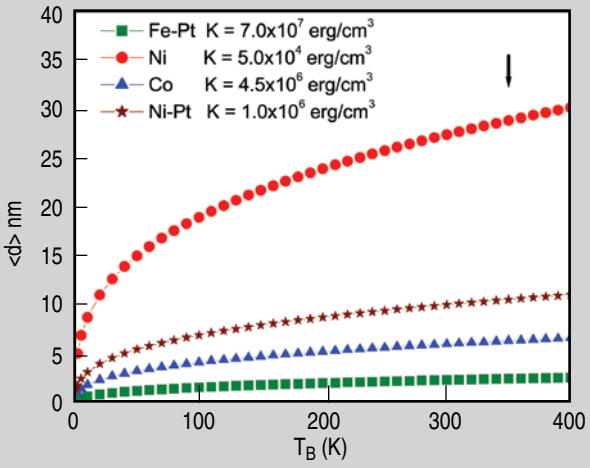

Figure 15. The variation of the blocking temperature (T_B) with the average diameter (<d>) of the Ni precipitates. An average size about 30 nm of Ni precipitates in MgO corresponds to a blocking temperature of 350 K as indicated by the arrow. For the sake of comparison, the plots of T_B vs. average size for other closely related systems, namely, FePt, Co and Ni-Pt nanodots, are also shown.

K with coercivity varying 6 (at 350 K) to 315 Oe (at 5 K). Detailed M (T) measurements under FC and ZFC conditions showed characteristic blocking temperatures, consistent with field dependent magnetization measurements. The FC and ZFC measurements were found to merge above the saturation fields ~5 kOe. Important parameters such as saturation magnetization (M_s), remnant magnetization (MR), coercive field (H_c) and the initial saturating field (H_s) calculated from the temperature-dependent magnetization of Ni-MgO showed a monotonic increase with the decrease in temperature as expected for noninteracting nanostructured magnetic systems.

References

1. C.L. Chien, *Annu. Rev. Mater. Sci.,* 25 (1995), p. 129.
2. J. Narayan et al., *Appl. Phys. Lett.,* 93 (2008), p. 082507.
3. S. Ramachandran et al., *Solid State Commun.,* 145 (2008), p. 18.
4. S. Ramachandran et al., *Appl. Phys. Lett.*, 87 (2005), p. 172502.
5. A. Tiwari et al., *Appl. Phys. Lett.*, 88 (2006), p. 142511.
6. J. Narayan and Y. Chen, *Phil. Mag.,* A, 49 (1984), p. 475.
7. M.M. Abraham, C.T. Butler, and Y. Chen, *J. Chem. Phys.*, 55 (1971), p. 3752.
8. J. Narayan, Y. Chen, and R.M. Moon, *Phys. Rev. Lett.*, 46 (1981), p. 1491.
9. S. Ramachandran, J.T. Prater, and J. Narayan, *Appl. Phys. Lett.* 90 (2007), p. 132511.
10. E.C. Stoner and E.P. Wohlfarth, *Philos. Trans. R. Soc. London, Ser.* A, 240 (1948), p. 599.
11. C. Kittel, *Introduction Solid State Physics,* 5th edition (New York: Wiley, 1976), p. 465.
12. R.H. Kodama, *J. Magn. Magn. Mater.,* 200 (1999), p. 359.
13. B.D. Cullity, *Introduction to Magnetic Materials* (Reading, MA: Addison-Wesley, 1972), pp. 117, 347 and 415.
14. G. Xiao and C.L. Chien, *J. App. Phys.,* 61 (1987), p. 3308.
15. S. Gangopadhyay et al., *Phys. Rev. B*, 45 (1992), p. 9778.
16. G. Xiao and C.L. Chien, *J. App. Phys.,* 63 (1988), p. 4252.
17. E.F. Kneller and F.E. Luborsky, *J. App. Phys.,* 34 (1963), p. 656.
18. A.H. Morrish, *The Physical Principles of Magnetism, ed.* (New York: Wiley. 1965).
19. J.L. Gittleman, B. Abeles, and S. Bozowski, *Phys. Rev. B,* 9 (1974), p. 3891.
20. H. Li et al., *IEEE Tans. Magn.*, 28 (1992), p. 3177.

J. Narayan, Sudhakar Nori, S. Ramachandran, and J.T. Prater are with the NSF Center for Advanced Materials and Smart Structures, Department of Materials Science and Engineering, North Carolina State University, Raleigh, NC 27695-7907, USA; J.T. Prater is also with the Materials Science Division, Army Research Office, Research Triangle Park, Durham NC 27709, USA. Dr. Nori can be reached at nsudhak@ncsu.edu.